PHYSICAL REVIEW C VOLUME 21, NUMBER 1 JANUARY 1980

Elastic and inelastic scattering of 162 MeV pions by ^{28}Si, ^{58}Ni, and ^{208}Pb

C. Olmer, D. F. Geesaman, B. Zeidman, S. Chakravarti, and T.-S. H. Lee
Argonne National Laboratory, Argonne, Illinois 60439

R. L. Boudrie
University of Colorado, Boulder, Colorado 80302
and Los Alamos Scientific Laboratory, Los Alamos, New Mexico 87544

R. H. Siemssen
Kernfysisch Vernsneller Instituut, Groningen, Netherlands

J. F. Amann, C. L. Morris, and H. A. Thiessen
Los Alamos Scientific Laboratory, Los Alamos, New Mexico 87544

G. R. Burleson and M. J. Devereux
New Mexico State University, Las Cruces, New Mexico 88001

R. E. Segel
Northwestern University, Evanston, Illinois 63301

L. W. Swenson
Oregon State University, Corvallis, Oregon 97331
(Received 17 May 1979)

Angular distributions for the elastic and inelastic scattering of 162 MeV π^+ and π^- by Si, ^{58}Ni, and ^{208}Pb have been measured. The elastic scattering data are fitted with optical model calculations in configuration space. Momentum-space optical-model calculations qualitatively reproduce the elastic scattering data, but substantially better agreement can be obtained if suitable modifications to the model are made. Distorted-wave impulse approximation calculations of the inelastic scattering, using both configuration-space and momentum-space models, generally reproduce the experimental data.

[NUCLEAR REACTIONS ^{28}Si(π,π'), ^{58}Ni(π,π'), ^{208}Pb(π,π'), $E=162$ MeV, measured $d\sigma/d\Omega$; optical potential and DWIA collective model analyses.]

I. INTRODUCTION

Studies of pion-nucleus elastic and inelastic scattering are already adding to our growing understanding of how the pion interacts with the nucleus. These studies are expected eventually to provide new insight into questions of nuclear structure which either cannot be readily answered using other probes of the nucleus or are more fruitfully studied using complementary probes. At incident energies between 100 and 250 MeV, pion-nucleus interactions are dominated by the broad $J=T=\frac{3}{2}$, $\Delta(1232)$ resonance in the pion-nucleon system. Only recently, however, has it become feasible to perform pion scattering experiments in this energy range with an energy resolution sufficient to allow the identification of transitions to individual levels in a wide range of nuclei.

For many years, the sole set of both elastic and inelastic pion scattering data was that of Binon *et al.*,[1] who investigated π^- scattering by ^{12}C at several energies between 120 and 260 MeV. More recently, new high-quality elastic and inelastic scattering data have appeared from research programs at the SUSI facility at SIN and at the EPICS facility at Clinton P. Anderson Meson Physics Facility (LAMPF) (e.g., Refs. 2–10). The strong energy dependence of the pion-nucleon interaction would indicate that a systematic study of both π^+ and π^- scattering at a particular incident energy by a variety of target nuclei would be a useful and important addition to this body of knowledge.

The present work addresses this need and involves a study of the elastic and inelastic scattering of both π^+ and π^- by Si, ^{58}Ni, and ^{208}Pb at an incident energy of 162 MeV. A preliminary analysis of the elastic scattering data has been reported previously,[10] together with the predictions of a parameter-free, momentum-space calculation. The failure of the theory to accurately reproduce

the elastic scattering data is discussed in more detail in the present paper, and modifications to the basic formalism of the model are suggested which substantially improve the agreement between the theoretical and experimental results. Analyses of the inelastic scattering data indicate that predominantly low-lying, collective states in these nuclei are populated. Predictions of a parameter-free, momentum-space, collective model are presented. Again, modifications to the model appear to be necessary in order to reproduce the data. However, both elastic and inelastic scattering calculations can be brought into agreement with the data by the same modification, namely a well-prescribed readjustment of the calculated local energy in the transformed pion-nucleon system which reflects both Coulomb and binding energy effects neglected in the original model. Alternative analyses of the elastic and inelastic scattering data with calculations using a Kisslinger optical potential are also discussed. The parameters of the interaction are adjusted to achieve optimum fits to the elastic scattering data. These results are then used in collective model distorted-wave impulse approximation (DWIA) calculations of the inelastic scattering.

II. EXPERIMENTAL PROCEDURE

The experiment was performed at the EPICS facility at LAMPF. A detailed description of the system is presented elsewhere.[11] Briefly, it consists of a pion channel which provides a vertically dispersed beam on target and a magnetic spectrometer composed of magnetic dipoles, bending in the vertical plane, which are preceded by a magnetic quadrupole triplet. The trajectories of the particles passing through the spectrometer are determined using multiwire counters located between the dipoles and triplet, as well as after the dipoles. This system thus permits the measurement of incident pion energy, emergent pion energy, and scattering angle. Consistency checks in the event by event analysis system also allow for the rejection of a major fraction of the muon events resulting from pion decay within the spectrometer.

In these measurements, the incident pion energy was 162.6 MeV, with an average flux on target of $\sim 5\times10^{7}$/sec for π^+ and $\sim 1\times10^{7}$/sec for π^-. The total momentum spread of the beam was $\sim\pm1\%$, with a point resolution $\Delta p/p$ of $\approx 2\times10^{-4}$. The π^+ scattering data were measured between 13.4° and 110° in 2.4° steps; the π^- were measured between 15.8° and 96.8° in 2.4° steps at forward angles ($\theta < 36°$) and in 3.6° steps at larger angles ($\theta > 36°$). The central 2.4° of the spectrometer angular acceptance was divided into separate 1.2° bins for analysis of the elastic scattering data. Limited inelastic scattering yields required the use of the full 2.4° acceptance for analysis of the inelastic scattering data. The angular resolution of the system was observed to be ~0.6°, and the angular setting of the spectrometer was determined to be accurate to within 0.2° by measurements near 0° with reduced beam intensity.

The targets used in the experiment were isotopically enriched metal foils of ^{58}Ni (292 mg/cm^2) and ^{208}Pb (289 mg/cm^2) and plates of natural Si (366 mg/cm^2, 92.2% ^{28}Si). The target size exceeded the beam spot (16 cm×6 cm). Energy spectra for the scattering of π^+ from each of these targets are shown in Fig. 1. The observed energy resolution of ~350 keV was limited by target thickness. This resolution is more than adequate for

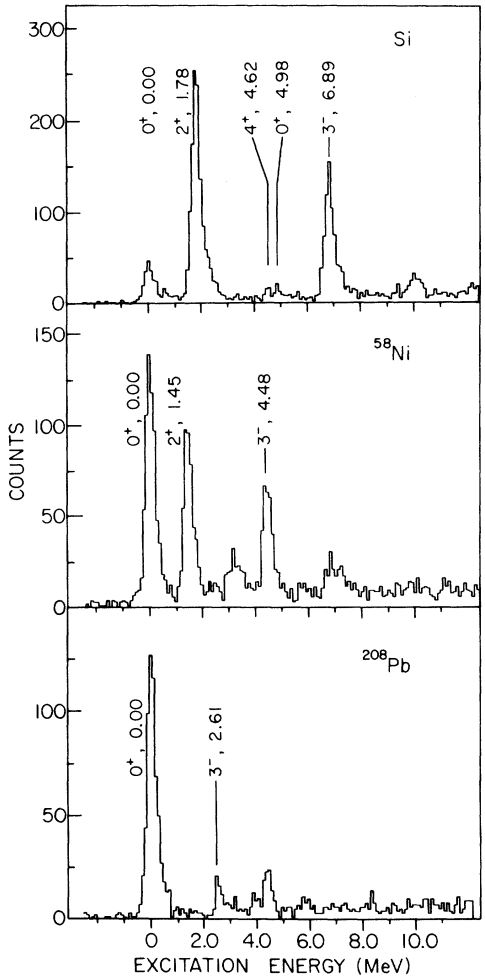

FIG. 1. Energy spectra obtained for the scattering of 162 MeV π^+ by Si, ^{59}Ni, and ^{209}Pb at laboratory angles of 38.0°, 30.8°, and 40.4°, respectively.

completely resolving the ground state from excited state transitions and allows clear separation of the strongly excited transitions at low excitation energies where the level density is small. Radiative effects[12] are apparent with the present energy resolution and contribute a small low-energy tail to the peak shape.

Relative differential cross sections were obtained by normalization to the pion flux measured with an ionization chamber situated at 0° downstream of the target. This normalization agrees with an alternative normalization based upon the total flux measured at the primary pion production target. The absolute normalization of the cross section is based on a comparison of pion scattering from carbon and hydrogen targets at the same energy (162.6 MeV), where carbon differential cross sections[13] have been accurately determined relative to pion-hydrogen scattering.[14] The earlier publication of the elastic scattering data[10] employed an alternative absolute normalization, based on another measurement[15] of pion-carbon elastic scattering, which resulted in a 10% increase in the π^+ normalization relative to the present value, and yielded a π^- normalization which is consistent, within combined errors with that presently used. The uncertainty in the absolute cross sections in the present work is estimated to be less than ±10%, subject to the additional uncertainty in the reference cross sections, while the relative cross sections are accurate to better than ±5%, ignoring purely statistical errors. Corrections for pion decay are included, but corrections owing to radiative effects[12] are estimated to be only a few percent and have not been included.

III. EXPERIMENTAL RESULTS

Angular distributions for the elastic scattering of 162.6 MeV π^+ and π^- by Si, ^{58}Ni, and ^{208}Pb are displayed in Figs. 2 and 3. Pronounced oscillatory structures are observed in the data and are characteristic of the strong pion absorption (i.e., removal of flux from the elastic channel) expected in the region of the (3, 3) resonance. Inspection of these angular distributions indicates relatively small differences in the peak-to-valley ratios for π^+ and π^- scattering from each of the targets and progressively larger shifts in oscillation frequency as the target mass is increased. Shifts in the oscillation frequency between π^+ and π^- angular distributions also become larger as the target mass is increased and primarily result from Coulomb effects, as can be shown by optical-model calculations which neglect the Coulomb interaction.

An estimate of where the pion interaction and

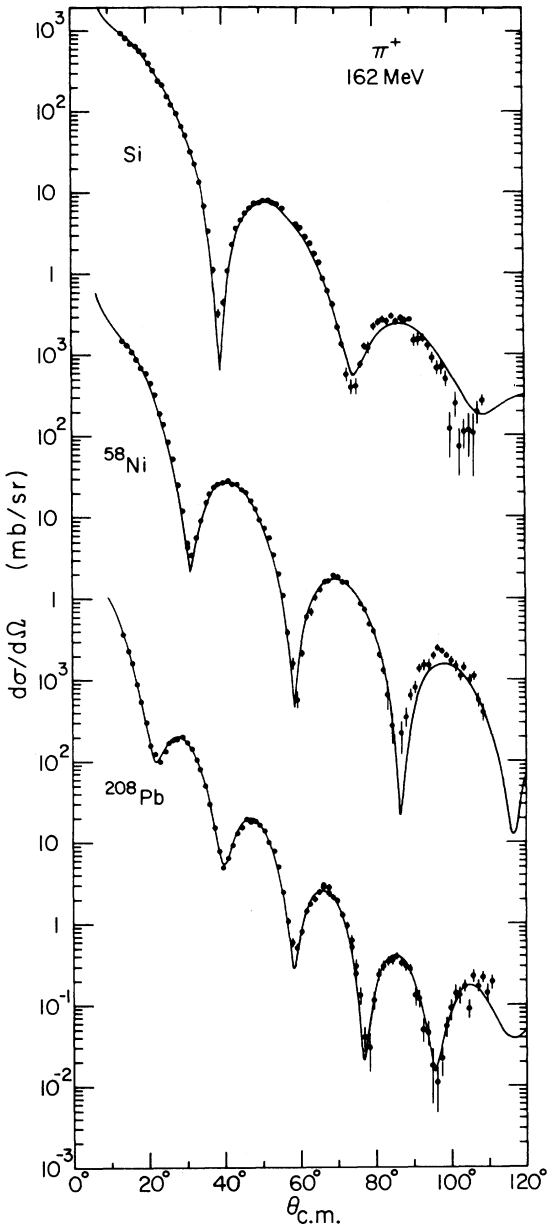

FIG. 2. Angular distributions for the elastic scattering of 162 MeV π^+ by Si, ^{58}Ni, and ^{208}Pb. The curves result from fits to the data using the optical-potential program FITPI.

subsequent absorption occurs in the nucleus can be obtained from an analysis of the elastic scattering data using a simple strong absorption model.[16] Here, the oscillation pattern is given by $J_1^2(qR)$, where q is the momentum transfer $[q = 2k \sin(\theta/2)]$, R is an effective radius, and J_1 is a Bessel function of order one. In this analysis, only the first two minima of each angular distribution were considered. The minima locations of the π^+ and

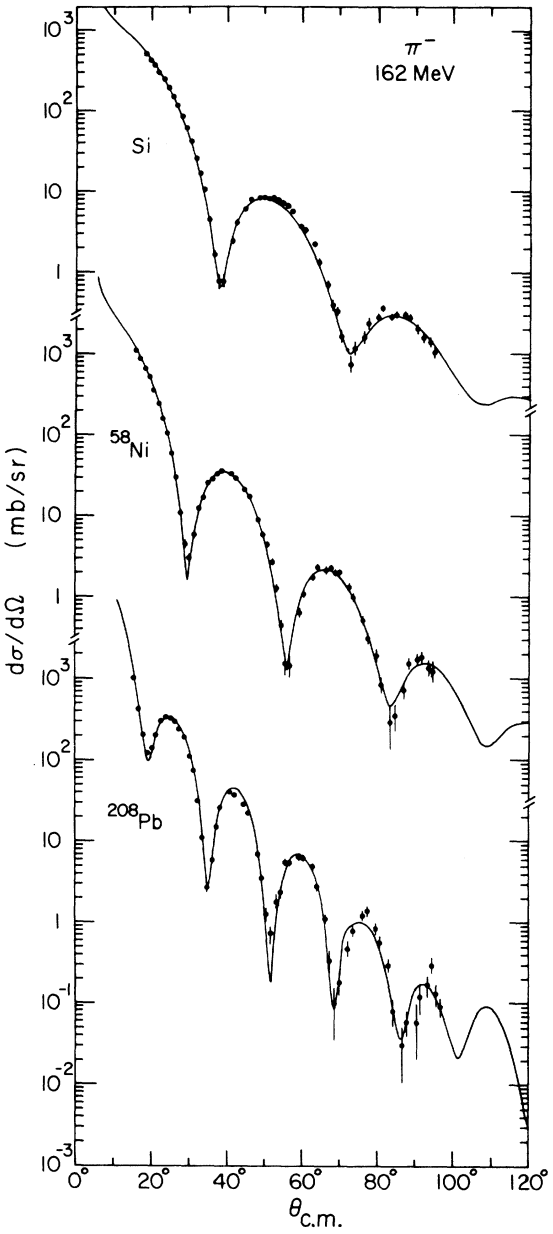

FIG. 3. Angular distributions for the elastic scattering of 162 MeV π^- by Si, ^{58}Ni, and ^{208}Pb. The curves result from fits to the data using the optical-potential program FITPI.

π^- angular distributions for each target were averaged in order to approximately remove Coulomb effects. The resulting effective radii are ~1.3 fm larger than the experimentally known half-density radii, as is characteristic for the scattering of strongly absorbed particles. For reasonable matter distributions (e.g., the charge distributions[17] determined by electron scattering experiments), the resulting densities at the effective radii are estimated to be less than 10% of the central density. Similar conclusions also result from an evaluation of the pion mean free path.[18] All of these considerations indicate that pion scattering near resonance is dominated by strong absorption and that the pions probe only the region of low nuclear density, i.e., the tail region of the density distribution where $\rho/\rho_0 \lesssim 10\%$.

More quantitative analyses using a first-order optical potential model have been applied to the elastic scattering data. In Secs. III A and III B, both coordinate-space calculations which adjust parameters in order to fit the data and momentum-space calculations with no free parameters are presented and compared to the data. The necessity for adjusting parameters in the latter analysis is found; prescriptions for these modifications and their physical bases are presented and discussed.

A. Configuration-space elastic scattering calculations

Configuration-space optical-model calculations of the elastic scattering were performed using the code FITPI.[19] An optical potential of the Kisslinger form[20] was employed,

$$2EV(\vec{r}) = -Ak^2 b_0 \rho(\vec{r}) + Ab_1 \vec{\nabla} \cdot \rho(\vec{r}) \vec{\nabla},$$

where $\rho(\vec{r})$ is the nuclear matter density and the complex parameters b_0 and b_1 were adjusted to obtain a least-squares fit to the data with the uncertainty in the absolute normalization of the data not included in the fit. The charge distributions were assumed to be of Woods-Saxon form, with parameters determined by electron scattering studies[17] and are listed in Table I. The matter distributions were also assumed to be of Woods-Saxon form, with identical parameters specifying proton and neutron distributions. The parameters (R, a) describing the matter distributions were chosen either (1) to be the same as those of the charge distributions, with a correction made for the finite charge radius of the proton, or (2) to vary in order to obtain a least-squares fit to the data. For each target, the π^+ and π^- scattering data were treated either separately or together. The resulting best-fit values of b_0 and b_1, together with the corresponding errors derived by the fitting program, are presented in Table I. Quantities which were held fixed during the fit are underlined in the table. For comparison, the values of b_0 and b_1 deduced from the free pion-nucleon phase shifts[21,22] are listed in Table II. As is indicated in the final column of this table, calculations using these values result in quite poor agreement with the data. Angular distributions calculated assuming

TABLE I. Optical potential parameters used in the FITPI calculations.

Nucleus	Data	R [a]	a [a]	Re(b_0) [b]	Im(b_0) [b]	Re(b_1) [b]	Im(b_1) [b]	χ^2/point
Si	π^+	2.82	0.55	−0.8 ± 0.3	1.3 ± 0.2	7.3 ± 0.3	5.9 ± 0.2	5.9
		2.71 ± 0.09	0.51 ± 0.01	−1.9 ± 1.6	0.1 ± 0.2	9.9 ± 0.6	8.4 ± 0.6	1.6
	π^-	2.82	0.55	−0.9 ± 0.3	1.7 ± 0.2	6.3 ± 0.3	6.1 ± 0.2	2.0
		2.86 ± 0.41	0.54 ± 0.04	−0.9 ± 0.4	1.6 ± 0.9	6.4 ± 1.9	6.2 ± 2.1	1.5
	π^+,π^-	2.82	0.55	−0.9 ± 0.3	1.7 ± 0.2	6.8 ± 0.3	6.3 ± 0.2	5.1
		2.54 ± 0.12	0.53 ± 0.01	−1.9 ± 0.2	−0.04 ± 0.3	10.3 ± 0.7	9.4 ± 0.7	2.8
^{58}Ni	π^+	3.97	0.54	1.4 ± 0.3	0.9 ± 0.2	4.7 ± 0.3	6.4 ± 0.2	3.9
		3.56 ± 0.08	0.55 ± 0.01	−0.5 ± 0.3	−1.2 ± 0.3	9.8 ± 0.8	10.1 ± 0.7	2.6
	π^-	3.97	0.54	−1.0 ± 0.5	1.3 ± 0.3	6.0 ± 0.5	6.4 ± 0.3	3.4
		3.09 ± 0.35	0.61 ± 0.02	−0.3 ± 0.9	−0.7 ± 1.5	10.0 ± 0.2	12.5 ± 3.5	2.7
	π^+,π^-	3.97	0.54	1.3 ± 0.3	0.9 ± 0.2	4.6 ± 0.2	6.4 ± 0.2	4.7
		3.33 ± 0.11	0.58 ± 0.01	0.13 ± 0.33	−1.5 ± 0.5	9.9 ± 1.0	11.8 ± 1.0	3.8
^{208}Pb	π^+	6.51	0.55	−0.6 ± 0.1	−1.2 ± 0.1	6.4 ± 0.2	6.4 ± 0.2	2.6
		6.53 ± 0.13	0.57 ± 0.02	0.2 ± 0.3	−1.0 ± 0.3	5.2 ± 0.8	6.3 ± 0.7	2.2
	π^-	6.51	0.55	−3.1 ± 0.6	−0.4 ± 0.5	9.3 ± 0.6	9.4 ± 0.5	4.0
		6.31 ± 0.37	0.66 ± 0.02	0.3 ± 1.4	2.9 ± 2.2	4.5 ± 2.2	6.8 ± 4.1	2.4
	π^+,π^-	6.51	0.55	−0.7 ± 0.2	−1.7 ± 0.2	6.6 ± 0.3	7.4 ± 0.2	11.1
		6.91 ± 0.15	0.55 ± 0.03	1.0 ± 0.2	−0.3 ± 0.4	2.6 ± 0.6	5.0 ± 0.7	7.7

[a] Underlined quantities held fixed during fit. The values of R and a are deduced from electron scattering studies (Ref. 17) with the relations $\langle r^2\rangle_{el} = \langle r^2\rangle_{charge} - (0.8)^2$ and $\frac{5}{3}\langle r^2\rangle = R^2 + \frac{7}{3}\pi^2 a^2$.
[b] Units are fm^3.

the fixed matter distributions and separate fitting of the π^+ and π^- data are displayed in Figs. 2 and 3.

Several observations concerning the best-fit parameters of Table I are noteworthy.

(a) Somewhat better fits to the data are obtained when the parameters of the matter distribution are allowed to vary. The preferred values of the half-density radius R appear to be either similar to or smaller than the values inferred from the charge distributions.

(b) For elastic scattering from Si, as well as from ^{58}Ni, the values of b_0 and b_1 which best describe the data are similar for π^+ and π^- scattering, whereas, for elastic scattering from ^{208}Pb, somewhat different values of the parameters are needed to describe the π^+ as compared to the π^- data, as expected from parameters deduced using the free-nucleon amplitudes for nuclei with large neutron excess.

(c) There appears to be considerable scatter in the fitted values of b_0 and b_1 for the various targets, and no obvious pattern can be discerned which could be used to predict precisely the elastic scattering from other targets. [We note that this scatter is not removed if the number of fitting parameters is reduced, e.g., by fixing the values of Re(b_0) and Im(b_0) at the free pion-nucleon value.]

(d) Calculations using the values of b_0 and b_1 based on the free pion-nucleon amplitudes fail to reproduce the observed data, although the expected trend of $|b_1| \gg |b_0|$ does result from the present analysis. For several of the calculations, a negative, unphysical value of Im(b_0) was obtained. However, since Im(b_1) $\gg$ Im(b_0), the net creation of flux implied by the negative sign occurs deeply

TABLE II. Optical potential parameters used in the FITPI calculations with free pion-nucleon phase shifts averaged over isospin.

Nucleus	Data	R	a	Re(b_0^{free}) [a]	Im(b_0^{free}) [a]	Re(b_1^{free}) [a]	Im(b_1^{free}) [a]	(χ^2/point$_{free}$)
Si	π^+	2.82	0.55	−0.78	0.35	3.90	8.96	58.0
	π^-	2.82	0.55	−0.78	0.35	3.90	8.96	12.0
^{58}Ni	π^+	3.97	0.54	−0.74	0.35	3.83	8.80	151.0
	π^-	3.97	0.54	−0.81	0.35	3.97	9.11	7.7
^{208}Pb	π^+	6.51	0.55	−0.56	0.34	3.44	8.00	368.0
	π^-	6.51	0.55	−0.99	0.36	4.35	9.90	14.0

[a] Units are fm^3.

inside the nucleus, a region that contributes negligibly to the scattering in the presence of strong absorption.

(e) Our ability to obtain nearly equivalent fits to the data with rather different parametrizations of the matter distribution would indicate, as has been previously suggested,[23] that analyses which employ these fitting procedures cannot properly be used for determining nuclear matter distributions. However, we believe that simultaneous fits to the π^+ and π^- angular distributions are sensitive to differences between the proton and neutron distributions. This type of analysis could have been performed for the Si data, but not for the ^{58}Ni and ^{208}Pb data, since the isospin dependence of the interaction is not well determined. Therefore, we postpone such a discussion to Sec. III B 2 where a more fundamental treatment of the π-nucleon interaction is employed.

We conclude that the present elastic scattering data can be well reproduced by optical potentials of the Kisslinger form with adjustable parameters. While this form of the potential does include the important s- and p-wave contributions, it is known to have theoretical shortcomings, particlarly in the off-shell properties. Thus the failure in the present work to find systematic trends in the deduced values of b_0 and b_1 may simply reflect deficiencies in the model. However, as will be discussed in Sec. IV A, this method is directly applicable to the calculation of pion inelastic scattering.

B. Momentum-space elastic scattering calculations

First-order optical-model calculations were performed with the momentum-space elastic scattering code PIPIT.[24] In these calculations, the collision matrix[25] was calculated using free pion-nucleon phase shifts[22] and a model for off-shell extrapolation.[26] The effects of nucleon Fermi motion were neglected and Coulomb distortion effects were included in these calculations. The charge distributions were assumed to have a square-well form, with parameters given by electron scattering studies[17] and listed in Table III; the nuclear matter distributions were assumed to have a Woods-Saxon form.

Calculations of π^+ and π^- elastic scattering were first carried out assuming identical proton and neutron distributions as inferred from the charge distributions, and with a correction made for the finite charge radius of the proton. The resulting angular distributions are displayed in Figs. 4 and 5, and the corresponding parameters, identified by the label "Electron" are listed in Table III. While the shape and the magnitude of the data are reproduced reasonably well by these calculations, two significant discrepancies are (1) the predicted oscillation frequency is too rapid for both π^+ and π^- scattering and (2) the depths of the calculated minima are too shallow for π^+ scattering and too deep for π^- scattering. Finite angular resolution can tend to reduce the depth of experimental minima, but cannot result in deeper minima. Inasmuch as these initial calculations are based upon a first-order optical model with no adjustable parameters, disagreements between data and calculations are not surprising.

Since electron scattering analyses do not determine the neutron matter distribution, the constraint of equal proton and neutron parameters may not be valid. To investigate whether relaxation of this constraint could substantially improve the quality of the agreement between the data and theory, calculations were performed in which the parameters of the neutron distribution were allowed to vary and those of the proton distribution were held fixed to the values deduced from electron scattering studies. Improved agreement can be obtained if the calculations employ significantly different neutron distribution parameters for π^+ and π^- scattering. However, in no case was it possible to improve the agreement for both π^+ and π^- scattering from a given target using the same parameters of the neutron distribution. We

TABLE III. Matter distribution parameters for PIPIT calculations.

	Charge	Electron[a]			Modified[b]		
Nucleus	$\langle r^2\rangle^{1/2}$ (fm)	$\langle r^2\rangle^{1/2}$ (fm)	R (fm)	a (fm)	$\langle r^2\rangle^{1/2}$ (fm)	R (fm)	a (fm)
^{28}Si	3.10	2.99	2.82	0.55	2.80	2.47	0.55
^{58}Ni	3.76	3.67	3.97	0.54	3.52	3.68	0.55
^{208}Pb	5.50	5.44	6.51	0.55	5.34	6.26	0.60

[a] The values of R and a are deduced from electron scattering studies (Ref. 17) with the relations $\langle r^2\rangle_{el} = \langle r^2\rangle_{charge} - (0.8)^2$ and $\frac{5}{3}\langle r^2\rangle = R^2 + \frac{7}{3}\pi^2 a^2$.

[b] The values of R and a are chosen so that $\langle r^2\rangle_{mod} = \langle r^2\rangle_{charge} - (1.3)^2$ and a adjusted for optimum agreement with the data.

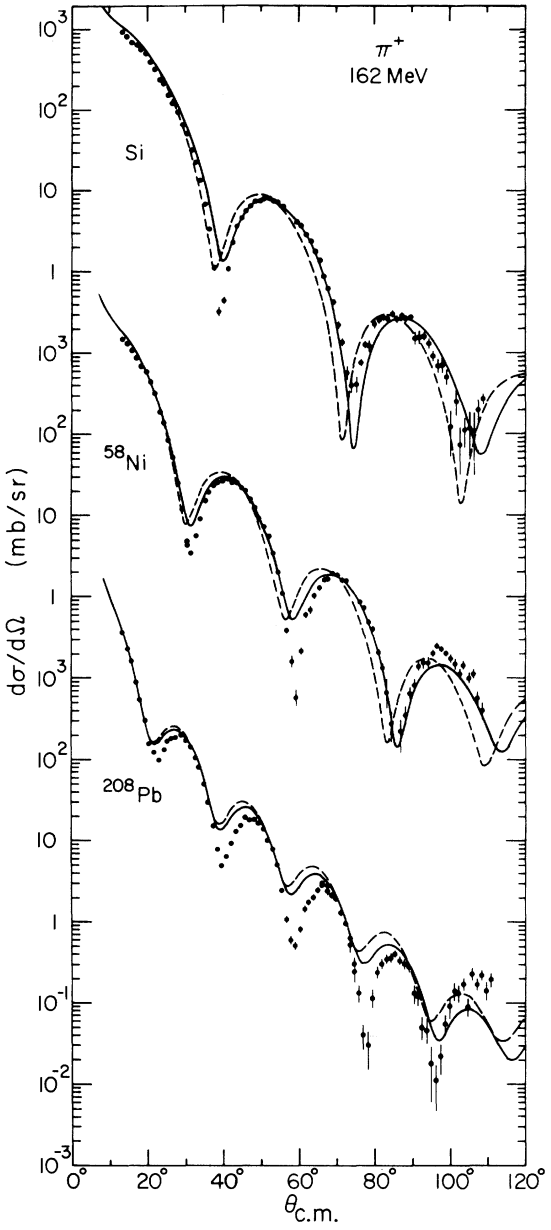

FIG. 4. Angular distributions for the elastic scattering of 162 MeV π^+ by Si, ^{58}Ni, and ^{208}Pb. The curves result from optical-potential calculations using the program PIPIT and assuming matter distribution radii deduced from electron scattering studies (dashed line) and radii modified from these values according to the prescription discussed in the text (solid lines).

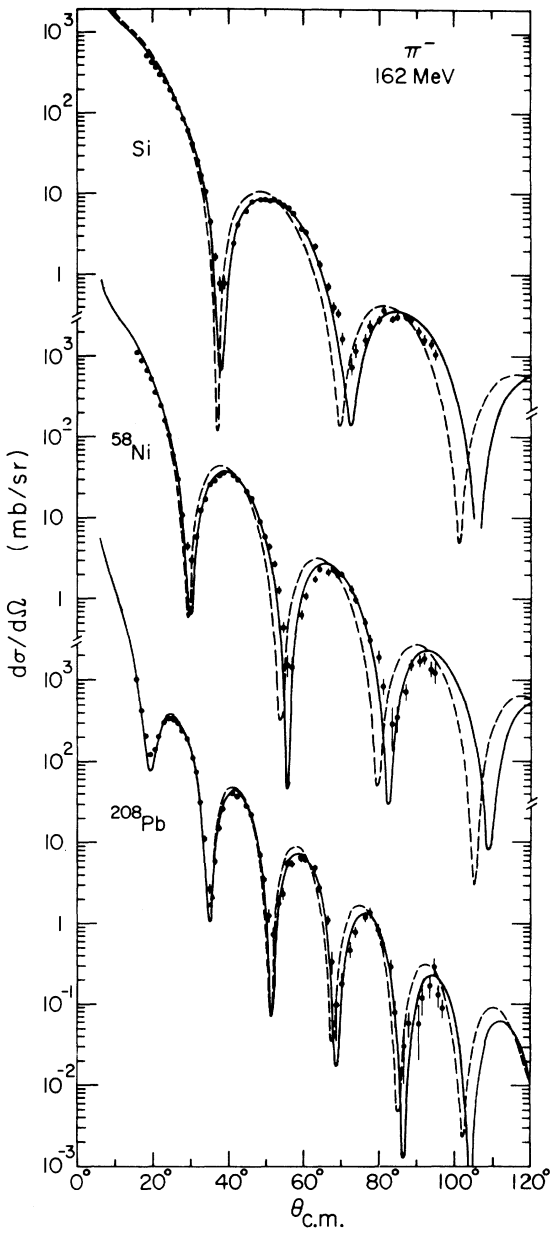

FIG. 5. Angular distributions for the elastic scattering of 162 MeV π^- by Si, ^{58}Ni, and ^{208}Pb. The curves result from optical-potential calculations using the program PIPIT and assuming matter distribution radii deduced from electron scattering studies (dashed line) and radii modified from these values according to the prescription discussed in the text (solid lines).

are therefore led to the conclusion that first-order PIPIT calculations with the assumptions noted earlier are not adequate for a detailed description of the elastic scattering data and that theoretical improvements are required.

1. Modifications to momentum-space calculations

The oscillation frequency in a strong absorption model is determined by the product of a radius and a momentum. The observed discrepancy be-

tween the data and calculations therefore suggests that the optical-model prescription employed so far apparently overestimates at least one of these parameters. For example, reasonably good agreement with the data is obtained for Si, ^{58}Ni, and ^{208}Pb calculations in which the proton and neutron rms radii are both artificially reduced by 1.3 fm from the charge rms radii, i.e.,

$$\langle r^2\rangle^{\text{mod}}_{\text{matter}} = \langle r^2\rangle_{\text{charge}} - (1.3)^2 ,$$

rather than by 0.8 fm as expected from the size of the proton charge. The resulting angular distributions are displayed in Figs. 4 and 5, and the corresponding parameters, identified by the label "modified," are listed in Table III. These calculations generally reproduce the oscillation frequency of each angular distribution, although the predicted minima depths exhibit the same problems discussed earlier. We note that the values of the matter distribution diffusivity used in the modified calculations are similar to those of the charge distribution for the Si and ^{58}Ni analyses, but for the ^{208}Pb analysis, substantially larger values of the diffusivity appear necessary in order to best reproduce the data.

In the preliminary analysis[10] of the data we noted that improved agreement between the data and calculations was observed if calculations were performed for pions of lower energy than were utilized in the experiment. While clearly invalid, these calculations may reflect certain physical effects that were neglected in the model and will be discussed in the remainder of this section.

The first effect to be considered is a shift in the pion kinetic energy owing to the Coulomb interaction. A positively-charged pion loses kinetic energy whereas a negatively-charged pion gains energy when it approaches a nucleus. Although PIPIT properly includes Coulomb effects in the evaluation of distortion effects in the partial wave distribution, the Coulomb energy correction is not ordinarily included in the evaluation of the pion-nucleon interactions. This latter effect was implemented in PIPIT by reducing the pion-nucleus collision energy in the pion-nucleus center of mass ω_0 by the Coulomb energy ΔE_{Coul}, i.e.,

$$\omega_0 = E_\pi(k_0) + E_A(k_0)$$
$$= (k_0^2 + M_\pi^2)^{1/2} + (k_0^2 + M_A^2)^{1/2}$$
$$(k_0^2 + M_\pi^2)^{1/2} + (k_0^2 + M_A^2)^{1/2} - \Delta E_{\text{Coul}}$$
$$= [(k_0')^2 + M_\pi^2]^{1/2} + [(k_0')^2 + M_A^2]^{1/2} ,$$

where, in the pion-nucleus center of mass, k_0 is the pion momentum and k_0' is the effective pion momentum including the presence of the Coulomb interaction. In the present work, the Coulomb energy corrections were calculated according to the prescription $\Delta E_c = \pm 1.44\, Ze^2/R$, where $R = 1.44\,(A^{1/3} + 0.55$ fm) and the sign of ΔE_{Coul} depends on the charge of the incident pion.

A second consideration arises because the optical potential calculated in PIPIT is constructed from a sum of pion-nucleon interactions obtained from free pion-nucleon phase shifts, i.e., the energy at which the pion-nucleon interaction is evaluated corresponds to a nuclear binding energy of zero. In the true nucleus, however, the nucleons are bound by many MeV and may be considered to have negative energies. Indeed it has been shown[27] that the effect of binding may be approximately included in the calculation by reducing the energy at which the pion-nucleon interaction is evaluated. Since the optical potential is generated by summing over all the nucleons in the nucleus, it is not immediately obvious that there is any simple way of accounting for binding. Near resonance, however, the pion interacts primarily with the surface, valence nucleons whose separation energy is simply the binding energy of the last nucleon. Moreover, on resonance, the π^+ plus proton and π^- plus neutron interaction strengths are three times the π^+ plus neutron and π^- plus proton strengths, respectively. Thus the net binding energy correction ΔE_{BE} may be approximated by the weighted average of the separation energies for the last proton (ϵ_p) and neutron (ϵ_n) of each nucleus, i.e.,

$$(\Delta E_{\text{BE}})\pi^+ = \tfrac{1}{4}(3\epsilon_p + \epsilon_n)$$
$$(\Delta E_{\text{BE}})\pi^- = \tfrac{1}{4}(3\epsilon_n + \epsilon_p) .$$

The pion-nucleon collision energy in the pion-nucleon center of mass $\tilde{\omega}_0$ was then reduced by the binding energy correction ΔE_{BE}, i.e.,

$$\tilde{\omega}_0 = E_\pi(\kappa_0) + E_N(\kappa_0)$$
$$= (\kappa_0^2 + M_\pi^2)^{1/2} + (\kappa_0^2 + M_N^2)^{1/2} ,$$
$$(\kappa_0^2 + M_\pi^2)^{1/2} + (\kappa_0^2 + M_N^2)^{1/2} - \Delta E_{\text{BE}}$$
$$= [(\kappa_0')^2 + M_\pi^2]^{1/2} + [(\kappa_0')^2 + M_N^2]^{1/2} ,$$

where, in the pion-nucleon center-of-mass system, κ_0 is the pion momentum and κ_0' is the effective pion momentum including the binding energy.

The values of ΔE_{Coul} and ΔE_{BE} used in the present work are listed in Table IV. While the binding energy corrections are roughly independent of target mass and pion charge ($\Delta E_{\text{BE}} \sim 10$ MeV), the effect of the Coulomb correction is to produce rather different values of ΔE_{Coul} for π^+ and π^- scattering from the various targets. Calculations were performed including the radius modification, as well as the binding and Coulomb corrections.

TABLE IV. Coulomb and binding energy correction parameters for PIPIT calculations.

Nucleus	ϵ_p [a] (MeV)	ϵ_n [a] (MeV)	$(\Delta E_{BE})\pi^+$ (MeV)	$(\Delta E_{BE})\pi^-$ (MeV)	$(\Delta E_c)\pi^+$ (MeV)	$(\Delta E_c)\pi^-$ (MeV)
^{28}Si	11.6	17.2	13.0	15.8	+3.89	−3.89
^{58}Ni	12.5	9.7	11.8	10.4	+6.32	−6.32
^{208}Pb	8.0	7.4	7.85	7.55	+12.65	−12.65

[a] Separation energy of last nucleon.

The resulting angular distributions are shown as the solid lines in Figs. 6 and 7. Calculations which assumed only (1) the radius modifications, (2) the radius modifications and binding energy corrections, and (3) the radius modifications and Coulomb energy corrections are shown by the dashed, dot-dashed, and dotted lines, respectively, in Figs. 6 and 7. The inclusion of the two energy corrections appears principally to alter the depths of the minima rather than to change the oscillation frequency. This effect is readily understood since, in the present situation of strong absorption, the faily large correction to the pion-nucleon energy implies a rather small effective distance in the nucleus and thus no obvious change in oscillation frequency.

Quite good agreement with the data is obtained with PIPIT when all three modifications are included in the calculations. The exception to this observation is for the $\pi^- + {}^{28}$Si data, where the calculation with only the radius modification produces better agreement. The necessity of including the energy corrections seems reasonable for we are taking into account, in a nearly parameter-free manner, two important physical effects which were previously neglected in the calculations. However, the necessity for reducing the matter distribution radii is not as well defined or understood. The modified radii could, of course, reflect the neglect of higher-order terms (e.g., ρ^2 terms) in the calculations, and thus could be expected to be energy and target dependent. An energy dependence of the binding energy correction might also be expected since, for kinetic energies far from the resonance, the pions may be able to probe deeper into the nucleus and to interact with more than just the valence nucleons. Analyses of elastic scattering data at lower and higher energies than considered here would be most instructive concerning these possible energy-dependent effects.

2. *Investigation of possible proton-neutron radius differences*

The relative success of these modified calculations in reproducing the π^+ and π^- elastic scattering angular distributions suggests further analyses to investigate possible differences between the proton and neutron radii, in particular for neutron-excess nuclei such as ^{208}Pb. Additional calculations, including the energy corrections, were carried out in which the neutron distribution parameters were varied from those of Figs. 6 and 7. The angular distributions for π^+ and π^- elastic scattering from ^{208}Pb are shown in Fig. 8, together with calculations in which the neutron radius was increased by 0.2 fm (solid line) and 0.1 fm (dashed line) and decreased by 0.1 fm (dotted line). As expected on resonance, the quality of agreement for π^+ scattering is relatively unchanged by the variation of neutron radius. However, a sensitivity to differences between proton and neutron radii is observed in the π^- calculations; whereas the quality of the fit is unaffected by radius differences as large as 0.1 fm, the agreement with the data becomes substantially poorer when the radius difference is 0.2 fm.

On the basis of the present optical-model calculations, we conclude that there is little, if any, difference in the proton and neutron densities in the vicinity of the strong absorption radius of Si, ^{58}Ni, and ^{208}Pb. These results are as expected for ^{28}Si and ^{58}Ni nuclei and, for ^{208}Pb, are consistent with other studies[28] of nuclear matter distributions which also indicate little or no difference in the neutron and proton radii. However, the results imply a disagreement with a recent analysis[29] of proton scattering at 800 MeV and with the theoretical matter distributions[30] deduced from density-dependent Hartree-Fock calculations. Since higher-order corrections may be sensitive to the neutron excess, a definitive interpretation of the present data must await improved model calculations. Moreover, pion scattering near the resonance energy, and hence the corresponding optical-model analyses, are sensitive only to the region of low nuclear density, where $\rho/\rho_0 \lesssim 10\%$. Thus, any conclusions concerning proton-neutron radius differences reflect only the tail of the density distributions and not regions closer to the nucleus (e.g., near the half-density radius). Since radius differences obtained from various experi-

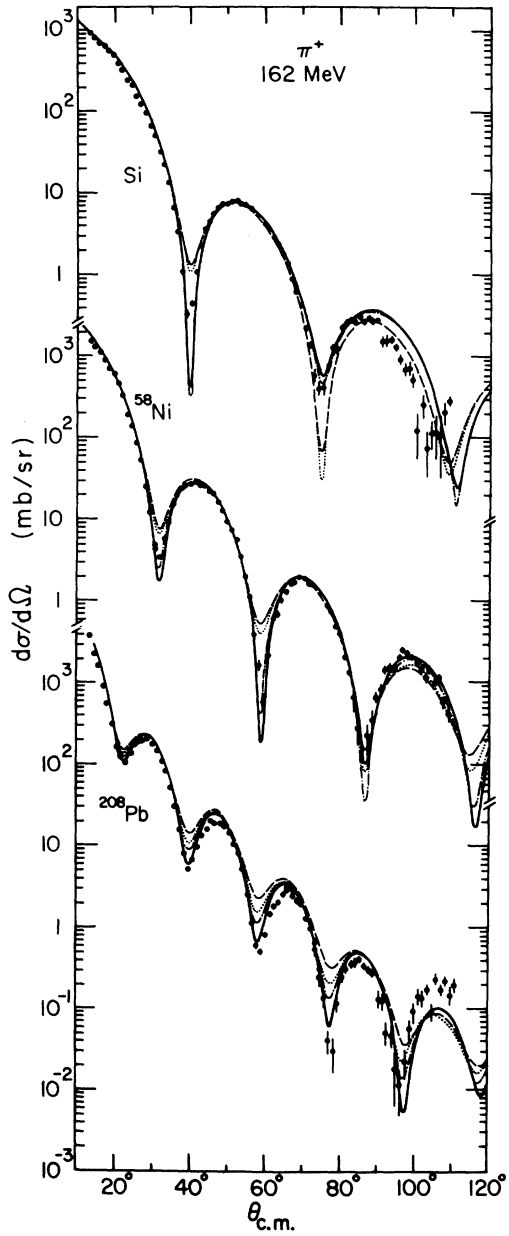

FIG. 6. Angular distributions for the elastic scattering of 162 MeV π^+ by Si, ^{58}Ni, and ^{208}Pb. The curves result from optical-potential calculations using the program PIPIT and the radius, Coulomb energy, and binding energy corrections (solid lines), the radius and Coulomb energy corrections (dotted lines), the radius and binding energy corrections (dot-dashed lines), and the radius correction alone (dashed lines).

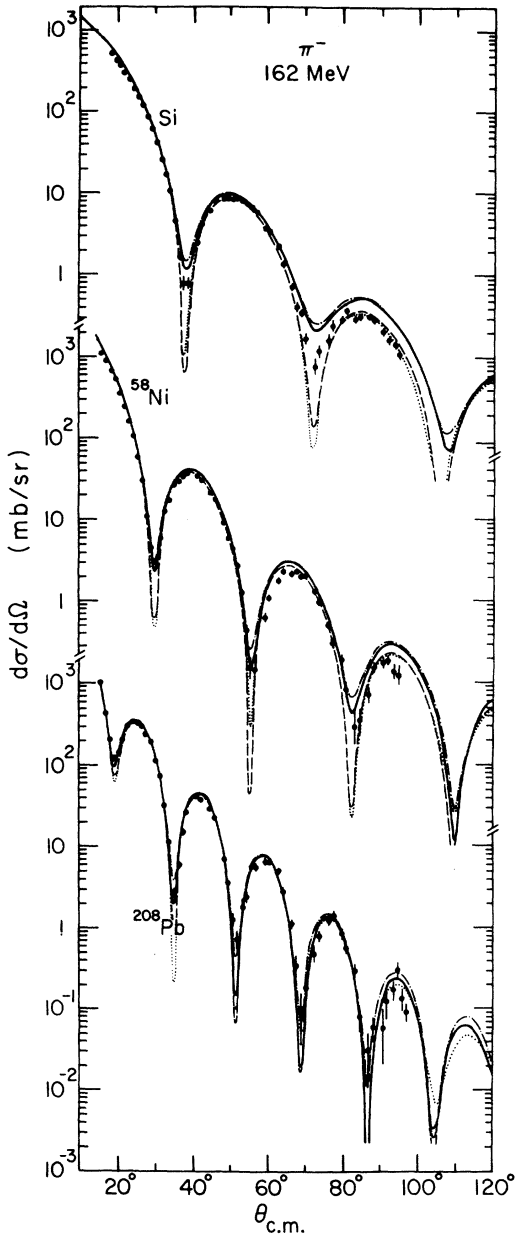

FIG. 7. Angular distributions for the elastic scattering of 162 MeV π^- by Si, ^{58}Ni, and ^{208}Pb. The curves result from optical-potential calculations using the program PIPIT and the radius, Coulomb energy, and binding energy corrections (solid lines), the radius and Coulomb energy corrections (dotted lines), the radius and binding energy corrections (dot-dashed lines), and the radius correction alone (dashed lines).

mental studies of weakly and strongly absorbing projectiles emphasize different reaction sensitivities, they many not be directly comparable.

IV. INELASTIC SCATTERING

One of the most important expectations from studies of pion inelastic scattering is the anticipated ability to extract proton and neutron nuclear structure information from comparisons of π^+ and π^- inelastic scattering. This is accomplished, at present, by obtaining the deformation probabilities

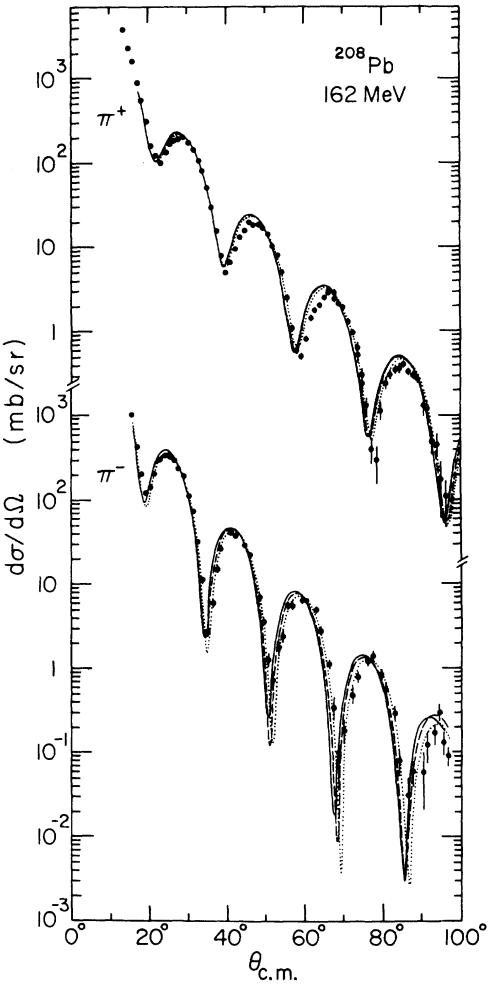

FIG. 8. Angular distributions for the elastic scattering of 162 MeV π^+ and π^- by ^{208}Pb. The curves result from optical-potential calculations using the program PIPIT and the radius, Coulomb energy, and binding energy corrections. The neutron distribution radii were assumed to be larger than the proton radii by 0.2 fm (solid lines) and 0.1 fm (dashed lines), and smaller than the proton radii by 0.1 fm (dotted lines).

β_L for the excitation of a state by both π^+ and π^- scattering and then employing various models to derive the proton and neutron structure information. Recently this method has been applied[5] in a study of pion scattering by ^{18}O, a nucleus in which the low-lying states are expected to have simple shell-model structures dominated by the presence of the two valence neutrons and thus to exhibit rather different π^+ and π^- scattering strengths. In other studies of pion inelastic scattering, e.g., by ^{24}Mg (Ref. 8) and ^{28}Si (Ref. 6), the predominant inelastic excitations involve low-lying, highly collective states, and thus only small differences are expected between π^+ and π^- scattering.

In the present work, several prominent peaks are observed in the pion spectra, as is indicated in Fig. 1. From a comparison of the π^+ and π^- data with inelastic scattering data using other projectiles, e.g., electrons, protons, and alpha particles, we identify these peaks with inelastic excitations of individual, known collective states in the target nuclei. Although these transitions are fairly well resolved over most of the angular range studied, the determination of inelastic yields is subject to significant errors because of uncertainties in the background due to (1) the often-intense low-energy tail of the elastic scattering peak, (2) the possible presence of weakly-excited, unresolved states, and (3) the possible presence of muon events (originating from pion decay) which are not completely rejected by the technique of reconstruction of particle trajectories. As a result, many inelastic data points are subject to more than 10% uncertainties in relative yield in addition to statistical errors and independent of the overall uncertainty in absolute normalization.

The angular distributions for the inelastic scattering of π^+ and π^- by ^{28}Si (1.78 MeV, 2^+; 4.62 + 4.98 MeV, $4^+ + 0^+$; 6.88 + 6.89 MeV, $3^- + 4^+$), ^{58}Ni (4.48 MeV, 3^-; 1.45 MeV, 2^+), and ^{208}Pb (2.61 MeV, 3^-) are presented in Figs. 9–11. In very recent, higher-resolution studies[31] of π^+ scattering by ^{28}Si, the inelastic transitions to the 4.62 MeV, 4^+ and 4.98 MeV, 0^+ levels could be resolved; the resulting limited angular distribution for the 4^+ level is displayed as the open circles in Fig. 9. In Fig. 12, we display the resolved 0^+ angular distribution. Strong oscillatory structures are apparent in the angular distributions, which are characteristic of the transferred angular momentum L and approximated by $J_L^2(kR)$ as in a strong absorption model.[16] A direct comparison of the π^+ and π^- data for each inelastic transition indicates frequency shifts between the π^+ and π^- data which are comparable to those observed in the elastic scattering data and principally caused by Coulomb effects. As a result, information concerning excitation probabilities and nuclear structure cannot be extracted from a simple comparison of π^+ and π^- inelastic scattering cross sections and require the use of theoretical models. In the following sections, calculations of the inelastic scattering are presented using both configuration-space and momentum-space codes which employ a collective model representation of the inelastic scattering form factor.

A. Configuration-space inelastic scattering calculations

The inelastic scattering of π^+ and π^- by ^{28}Si, ^{58}Ni, and ^{208}Pb has been calculated with the code

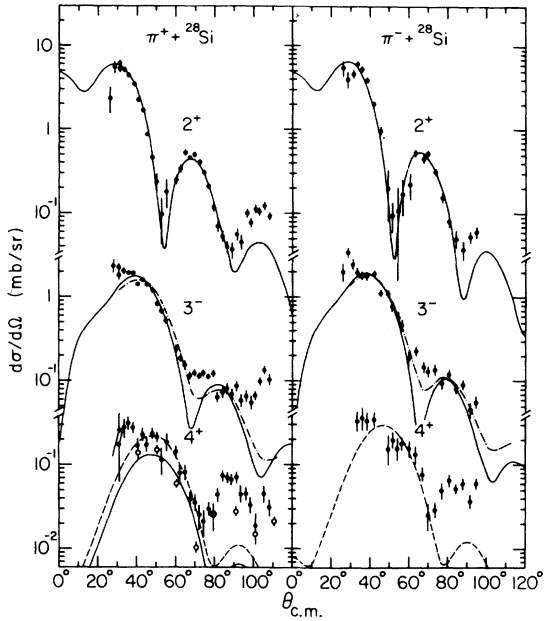

FIG. 9. Angular distributions for the inelastic scattering of 162 MeV π^+ and π^- to the 1.78 MeV, 2^+, 4.62 MeV, 4^+, and 6.88 MeV, 3^- states in ^{28}Si. The 4^+ angular distributions also contain yield from excitation of the 4.98 MeV, 0^+ level. The angular distribution for the resolved 4^+ excitation alone is displayed by the open circles. The various curves result from DWIA calculations discussed in the text using the program DWPI, normalized to the data with the parameters listed in Table V.

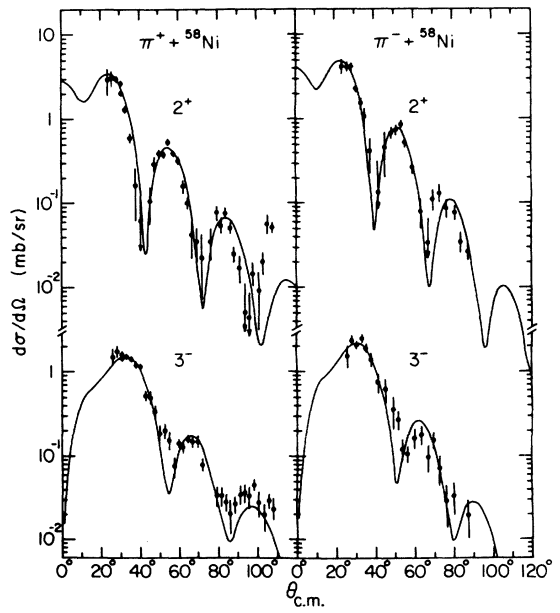

FIG. 10. Angular distributions for the inelastic scattering of 162 MeV π^+ and π^- to the 1.45 MeV, 2^+ and 4.48 MeV, 3^- states in ^{58}Ni. The curves result from DWIA calculations using the program DWPI and are normalized to the data with the parameters listed in Table V.

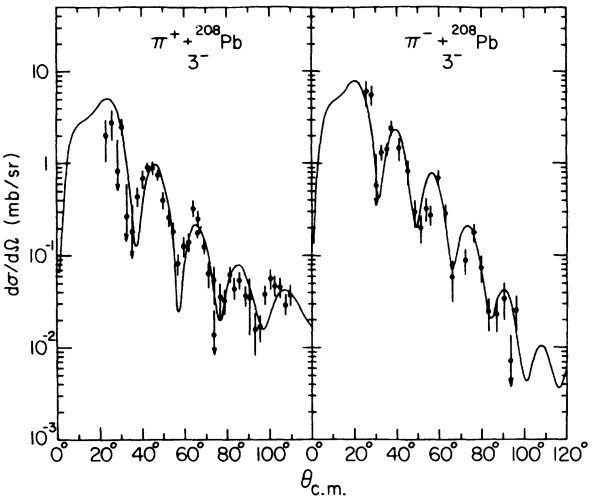

FIG. 11. Angular distributions for the inelastic scattering of 162 MeV π^+ and π^- to the 2.61 MeV, 3^- state in ^{208}Pb. The curves result from DWIA calculations using the program DWPI, and are normalized to the data with the parameters listed in Table V.

DWPI[32] which uses the distorted-wave impulse approximation (DWIA) and a macroscopic derivative form factor

$$\langle \Phi_{I'M'} | H | \Phi_{IM} \rangle = A t_{\pi N} \frac{\beta_L F_L(r)}{2L+1} ,$$

$$F_L(r) = r \frac{\partial \rho(r)}{\partial r} ,$$

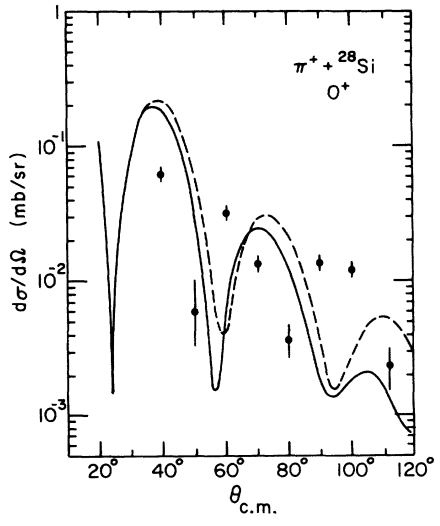

FIG. 12. Angular distribution for 162 MeV π^+ inelastic scattering to the 4.98 MeV, 0^+ state in ^{28}Si. The curves result from DWIA calculations using the program DWPI (solid curve, $\beta = 0.03$) and ARPIN (dashed curve, $\beta = 0.03$).

where conventional notation is used. The parameters of the calculations are listed in Table III. The distorted waves were generated using a Kisslinger potential and the parameters b_0 and b_1 obtained from separate fits to the π^+ and π^- elastic scattering data for each target, as discussed in Sec. III A. The matter distributions were assumed to be identical for protons and neutrons, with parameters deduced from electron scattering studies. Coulomb excitation was found to be unimportant for the inelastic scattering considered here. The resulting angular distributions are shown in Figs. 9–12 and the corresponding values of the deformation parameter β_L and deformation length $\beta_L R$ are listed in Table V. We note that the nuclear structure information is contained in the normalization factor $\beta_L{}^2$ required to bring the calculations into optimum agreement with the data.

The calculated angular distributions for both π^+ and π^- scattering to the 1.78 MeV, 2^+ level in ^{28}Si, 1.45 MeV, 2^+ level in ^{58}Ni, and 2.61 MeV, 3^- level in ^{208}Pb generally reproduce the experimental results, although the quality of the agreement deteriorates at large angles (greater than ~80°) for the ^{28}Si angular distributions. Rather poorer agreement is obtained for calculations of both π^+ and π^- scattering to the 4.48 MeV, 3^- level in ^{58}Ni and, in particular the 6.88 MeV, 3^- level in ^{28}Si. More oscillatory structure is predicted than is observed, although the general shapes of the angular distributions are well reproduced by the calculations. Since angular distributions for the well-resolved levels at low excitation energy exhibit more structure than seen for the states at high excitation energy, where the level density is also higher, one possible cause of this discrepancy could be that the experimental angular distributions contain additional yield from weakly excited and unresolved neighboring states, thereby tending to reduce the depths of the observed minima. In particular, the experimental angular distributions for the 6.88 MeV, 3^- level in ^{28}Si also include possible inelastic excitation to the nearby 6.89 MeV, 4^+, 7.38 MeV, 2^+, and 7.42 MeV, 2^+ states. Recent higher-resolution inelastic scattering studies indicate that these 2^+ states are only weakly excited (~10%) as compared to the combined excitation of the 3^- and 4^+ states, and do not affect either the shape or magnitude of the present data. The contribution of the unresolved 4^+ excitation to the observed angular distribution, however, could be substantial. Calculations were carried out for the combined excitation of the 6.88 MeV, 3^- and 6.89 MeV, 4^+ states, allowing the deformation parameters of the levels to vary in order to investigate the sensitivity of the resulting angular distribution to the 4^+ component. The dot-dashed curves in Fig. 9 show the calculated angular distribution assuming $\beta_3 = 0.41$ and $\beta_4 = 0.24$. [For comparison, and since the $B(E4)$ value for the 6.89 MeV, 4^+ state is not experimentally known, we note that the $B(E4)$ value[33] for the 4.62 MeV,

TABLE V. Deformation parameters from π^+ and π^- inelastic scattering.

Target	E_{ex} (MeV)	J^π	Beam	DWPI analysis β_L	DWPI analysis $\beta_L R$[a]	ARPIN analysis β_L	ARPIN analysis $\beta_L R$[b]	(e,e') β_L	Other reactions $\beta_L R$
^{28}Si	1.78	2^+	π^+	0.53 ± 0.02	1.49 ± 0.06	0.38 ± 0.02	0.94 ± 0.05	0.39[c]	1.1 –1.41[c]
			π^-	0.52 ± 0.02	1.47 ± 0.06	0.37 ± 0.02	0.91 ± 0.05		
	4.62	4^+	π^+[d]	0.24 ± 0.02	0.68 ± 0.06	0.28 ± 0.04	0.69 ± 0.10	0.10[c]	0.94–0.95[c]
			π^-[d]	0.25 ± 0.04	0.71 ± 0.11	0.28 ± 0.04	0.69 ± 0.10		
			π^+[e]	0.19 ± 0.02	0.54 ± 0.06	0.22 ± 0.02	0.54 ± 0.05		
	6.88	3^-	π^+	0.45 ± 0.02	1.27 ± 0.06	0.42 ± 0.02	1.04 ± 0.05		1.41[f]
			π^-	0.46 ± 0.02	1.30 ± 0.06	0.42 ± 0.02	1.04 ± 0.05		
^{58}Ni	1.45	2^+	π^+	0.21 ± 0.01	0.83 ± 0.04	0.14 ± 0.01	0.52 ± 0.04	0.19[g]	0.77–1.07[g]
			π^-	0.24 ± 0.01	0.95 ± 0.04	0.15 ± 0.01	0.55 ± 0.04		
	4.47	3^-	π^+	0.21 ± 0.01	0.83 ± 0.04	0.17 ± 0.01	0.63 ± 0.04	0.16[g]	0.60–0.89[g]
			π^-	0.23 ± 0.02	0.91 ± 0.08	0.19 ± 0.01	0.70 ± 0.04		
^{208}Pb	2.61	3^-	π^+	0.14 ± 0.01	0.91 ± 0.07	0.08 ± 0.02	0.50 ± 0.12	0.12[h]	0.52–0.95[h]
			π^-	0.14 ± 0.01	0.91 ± 0.07	0.13 ± 0.01	0.81 ± 0.06		

[a] $R(^{28}\text{Si}) = 2.82$ fm, $R(^{58}\text{Ni}) = 3.97$ fm, $R(^{208}\text{Pb}) = 6.51$ fm.
[b] $R(^{28}\text{Si}) = 2.46$ fm, $R(^{58}\text{Ni}) = 3.68$ fm, $R(^{208}\text{Pb}) = 6.26$ fm.
[c] Reference 33.
[d] Normalized to unresolved $4^+ + 0^+$ angular distribution, assuming excitation of 4^+ only.
[e] Normalized to resolved 4^+ angular distribution.
[f] Reference 34.
[g] Reference 35 and 36.
[h] Reference 35.

4^+ state in ^{28}Si implies that β_4 (4.62 MeV) = 0.23.] The contribution to the combined angular distribution from the unresolved excitation to the two 2^+ states was not included, but is estimated to increase the minima depths by only $\lesssim$10% and to be negligible at other angles. The agreement with the data is now significantly better than was obtained when assuming only a 3^- excitation. Although these calculations still cannot reproduce the experimental yields at angles greater than 100°, this problem is also present for calculations of inelastic scattering to other states.

Generally poor agreement between the calculated and experimental angular distributions is observed for both π^+ and π^- inelastic scattering to the 4.62 MeV, 4^+ and 4.98 MeV, 0^+ levels in ^{28}Si. The dashed curves in Fig. 9 are DWPI calculations assuming excitation of only the 4^+ level and normalizing to the present data (which can contain yield for both 4^+ and 0^+ excitation). The same calculation was normalized (solid curve) to the recent, high-resolution π^+ data (open circles) for inelastic scattering to the 4^+ state alone. It is evident that these calculations fail to reproduce the observed angular distributions for both π^+ and π^- scattering by (1) underpredicting the yield at angles greater than ~70° and (2) erring in the location of the minima experimentally observed near ~70°. The latter effect is not observed in DWPI calculations of the other transitions measured in the present work and thus could be specific to the nuclear structure of this state. Two-phonon excitation has been demonstrated to be an important contribution in inelastic alpha-particle scattering to the 4.62 MeV, 4^+ state. Thus it is possible that two-step processes are also important for pion scattering. Similar conclusions also result from analyses of the 0^+ excitation. The DWPI calculations, shown as the solid lines in Fig. 12, fail to reproduce the experimentally observed oscillation frequency.

The deformation parameters β_L and deformation lengths $\beta_L R$ extracted from this analysis are listed in Table V, together with the values obtained in inelastic scattering studies with other projectiles. In general, nearly identical parameters are deduced for π^+ and π^- scattering to a particular state. This result is expected for scattering from a $T = 0$ nucleus, such as ^{28}Si. For neutron-excess nuclei, such as ^{58}Ni and ^{208}Pb, differences in the deformation parameters for π^+ and π^- scattering can be interpreted in terms of different proton and neutron radii and/or deformations for excited states in nuclei. This procedure has been carried out for pion inelastic scattering by ^{18}O.[5] However, the present data indicate little, if any, evidence for such effects in the nuclear states studied here and will be discussed further in Sec. IV C.

The present values of β_L and $\beta_L R$ are in generally good agreement with those deduced from inelastic scattering studies with other projectiles, such as (α, α'), (d, d'), (p, p'), and (e, e'). However, two important points should be noted. First, a rather wide range in the values of β_L and $\beta_L R$ results from these other studies, and so the physical significance of such an agreement may be doubtful. Moreover, there are conceptual problems which affect any comparison of β_L and $\beta_L R$ for scattering by different projectiles. Inelastic scattering studies have indicated an ambiguity in the values of β_L and R such that different, equally valid values of β_L can exist for different radii R, and only the product $\beta_L R$ may be a well-determined quantity. However, the various projectiles are sensitive to quite different regions of the nucleus and, in addition, the pion potential is nonlocal. Therefore, a comparison of $\beta_L R$ for different projectiles may not be a physically meaningful approach.

B. Momentum-space inelastic scattering calculations

It has recently become feasible to perform inelastic pion scattering calculations in momentum space in a manner analogous to calculations of elastic scattering. In this section, we present results of calculations with the momentum-space inelastic pion scattering code ARPIN. A complete description of this program will appear elsewhere.[37]

These calculations employ the wave functions for elastic scattering calculated with PIPIT, using the radius and Coulomb and binding energy corrections discussed earlier. In these calculations, the macroscopic derivative form factor undergoes a Fourier transform to momentum space. As in other macroscopic models, the deformation parameter is used as a normalization factor and contains the nuclear structure information. (We again note that Coulomb excitation processes are not important here and can be neglected.)

Angular distributions for transitions to low-lying collective states in ^{28}Si, ^{58}Ni, and ^{208}Pb are shown in Figs. 12–15, together with the predictions calculated with ARPIN. Rather good agreement is obtained between calculated and experimental angular distributions for both π^+ and π^- inelastic scattering to the 2^+ and 4^+ states in ^{28}Si and the 2^+ state in ^{58}Ni, and for π^- scattering to the 3^- state in ^{208}Pb. In particular, the locations of the minima in the angular distributions are correctly reproduced by these calculations which include the radius modification discussed earlier.

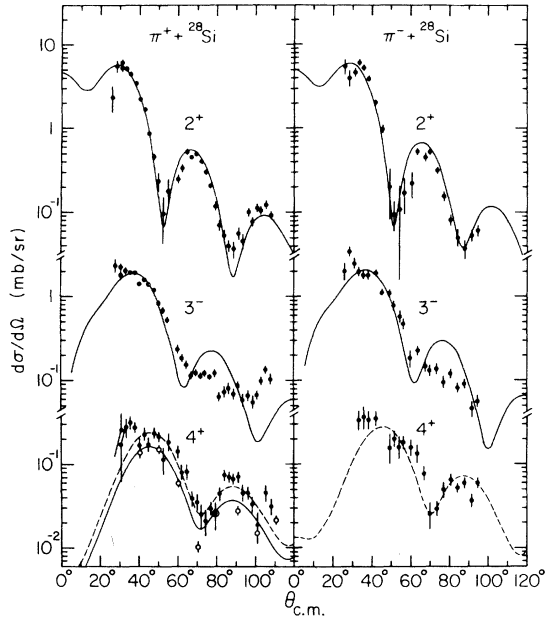

FIG. 13. Angular distributions for the inelastic scattering of 162 MeV π^+ and π^- to the 1.78 MeV, 2^+, 4.62 MeV, 4^+ and 6.88 MeV, 3^- states in ^{28}Si. The 4^+ angular distributions also contain yield from excitation of the 4.98 MeV, 0^+ level. The angular distribution for the resolved 4^+ excitation alone is displayed by the open circles. The various curves result from DWIA calculations using the program ARPIN, discussed in the text, normalized to the data with the parameters listed in Table V.

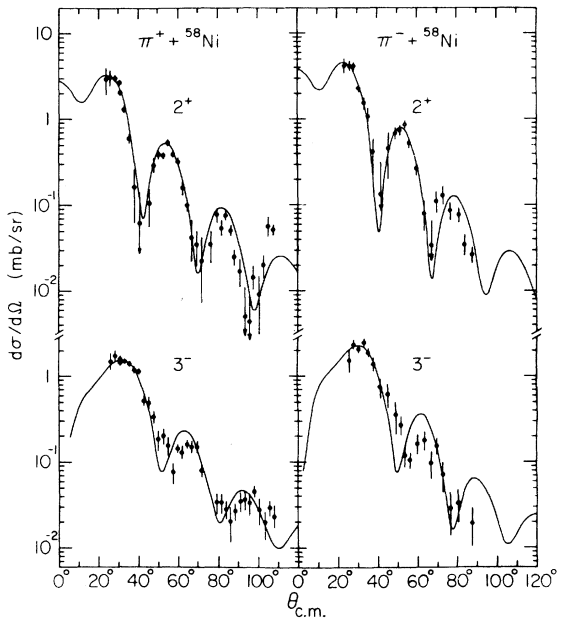

FIG. 14. Angular distributions for the inelastic scattering of 162 MeV π^+ and π^- to the 1.45 MeV, 2^+ and 4.48 MeV, 3^- states in ^{58}Ni. The curves result from DWIA calculations using the program ARPIN and are normalized to the data with the parameters listed in Table V.

On the other hand, inelastic scattering calulations which do not include this modification systematically fail to correctly predict the oscillation frequency, in a manner similar to that observed in the elastic scattering analyses.

The quality of the agreement between the calculations and the data is somewhat poorer for the remaining angular distributions. As was indicated in the previous section, such discrepancies for the 3^- transitions in ^{28}Si and ^{58}Ni may not be surprising as a result of possible excitation to nearby, unresolved levels. However, it is difficult to understand how such an explanation can account for the fact that the calculation for the ^{28}Si 3^- state overpredicts the cross sections at back angles.

Further discrepancies between the calculated and experimental angular distributions are present for excitation of the 4.98 MeV, 0^+ level in ^{28}Si. The calculated oscillation frequency is significantly smaller than is actually observed. Similar observations were made for DWPI analyses of both the 4^+ and 0^+ data and suggested the importance of two-step processes. Analyses with ARPIN, however, are able to reproduce the 4^+ data, and problems remain only for the 0^+ calculations. Thus, deficiencies present in one model and absent in another may account for the discrepancies

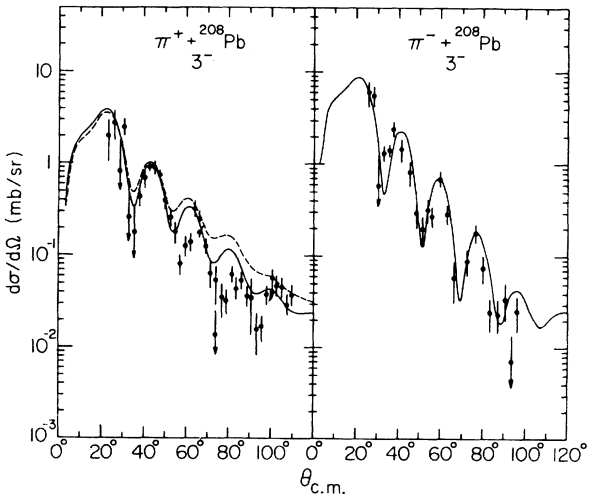

FIG. 15. Angular distributions for the inelastic scattering of 162 MeV π^+ and π^- to the 2.61 MeV, 3^- state in ^{208}Pb. The various curves results from DWIA calculations using the program ARPIN, discussed in the text, and are normalized to the data with the parameters listed in Table V.

encountered in analyses of the 4^+ excitation. The possibility that two-step processes are indeed important for the 0^+ excitation is currently under investigation. The failure of the calculations to reproduce the π^+ inelastic scattering to the 3^- level in ^{208}Pb is not at all understood. Although the locations of the minima are fairly well reproduced, the observed peak-to-valley ratios are significantly larger than predicted by ARPIN. This is reminiscent of what was found for momentum-space calculations of elastic scattering, which did not include the Coulomb and binding energy corrections. In fact, a calculation of the inelastic scattering in ^{208}Pb which neglects these corrections is shown by the dashed lines in Fig. 15. Clearly, such corrections have a large effect on the calculated angular distributions, but further corrections appear to be necessary.

The values of the deformation parameters β_L and deformation lengths $\beta_L R$ extracted from this analysis are presented in Table V. As in the DWPI analyses, nearly identical values of β_L are obtained for π^+ and π^- scattering to a particular state. The exception to this observation for pion scattering to the 3^- level in ^{208}Pb may not be significant in view of the rather poor agreement between calculations and data for π^+ scattering. As in the DWPI analyses, the values of β_L and $\beta_L R$ for pion scattering are generally in good agreement with those resulting from inelastic scattering studies using other projectiles. However, the same considerations concerning the significance of such a comparison which were discussed in Sec. IV A would also apply here.

C. Discussion

In the preceding two sections, calculations were presented for pion inelastic scattering using configuration-space (DWPI) and momentum-space (ARPIN) codes, both of which employed a DWIA approach with a collective form factor. The elastic scattering counterparts of these two models (FITPI and PIPIT, respectively) produced fits of comparable quality to the elastic scattering data. Since different π-nucleus interactions are used in these models, a comparison of the predicted shapes and extracted normalization factors β_L for the two sets of calculations may be instructive.

From inspection of the angular distributions calculated using DWPI and ARPIN for each of the observed excitations in ^{28}Si, it is apparent that larger oscillation frequencies are predicted with ARPIN. The predicted minima locations for the ARPIN calculations systematically occur at smaller angles than for the DWPI calculations. For the 2^+ transition, this difference in frequency is somewhat small (~2° at the minimum near ~50°), but becomes larger with increasing multipolarity of the transition (~8° for the minimum near 80° in the 4^+ angular distribution). A similar effect is also present for the ^{58}Ni calculations and is more pronounced for the 3^- angular distributions. In addition, it is evident that the magnitude of the difference is larger for π^+ than for π^- scattering. On the other hand, a comparison of the ^{208}Pb calculations indicates that the oscillation frequency for the ARPIN result is larger for π^+ scattering and smaller for π^- scattering than the frequency calculated with DWPI. Since configuration- and momentum-space calculations necessitate different treatments of the Coulomb interaction, any differences in these treatments could be manifested in the predicted oscillation frequency. However, it is difficult to reconcile this explanation with the observation that the differences in predicted oscillation frequency are larger for (1) inelastic scattering from ^{28}Si than from ^{208}Pb and (2) inelastic scattering to states of higher spin (e.g., the 4.62 MeV, 4^+ state in ^{28}Si than to lower spin states. An alternative origin of this effect could arise from the use of different π-nucleus interactions in the two calculations. The quality of the fits to the inelastic scattering data is, however, not sufficient to permit a definitive statement concerning the relative success of the two methods.

Further differences between the configuration- and momentum-space calculations are evident from a comparison of the extracted values of β_L. Smaller values of β_L are obtained from the ARPIN calculations than from the DWPI calculations. Since the matter distribution radii which were employed in the calculations were also smaller for ARPIN than for DWPI, considerable differences are observed in the values of $\beta_L R$ determined by the two methods. The significance, if any, of these differences in β_L and $\beta_L R$ is not clear at present.

The extraction of β_L for both π^+ and π^- inelastic scattering presents the opportunity of investigating possible differences in the proton and neutron distributions in neutron-excess nuclei. For example, the presence of two extra neutrons in the ^{58}Ni $T=1$ nucleus might be expected to result in substantially different values of $\beta_L(\pi^+)$ and $\beta_L(\pi^-)$, as has been observed for ^{18}O. However, the shell closure at $A=56$ is far from complete and the 2^+ and 3^- states in ^{58}Ni are rather collective. This may be seen in the need for large effective charges in shell-model calculations for this nucleus. Thus, excitation of both proton and neutron particle-hole configurations are equally likely, and no significant differences between $\beta_L(\pi^+)$ and $\beta_L(\pi^-)$

are expected for scattering to either the 2^+ or 3^- state in ^{58}Ni. The values of β_L and $\beta_L R$ deduced in the present work for ^{58}Ni are listed in Table V. These values indicate little, if any, enhancement of $\beta_L(\pi^-)$ relative to $\beta_L(\pi^+)$ and so are in agreement with the expectation that the two valence neutrons have little effect on the excitation probability.

Differences in the values of β_L deduced for π^+ and π^- inelastic scattering could possibly also be present for the 3^- state in ^{208}Pb. Whereas $\beta_3(\pi^-)/\beta_3(\pi^+) \approx 1.0$ results from the DWPI analysis, the ARPIN analysis indicates that $\beta_3(\pi^-)/\beta_3(\pi^+) \approx 1.5$. For the latter calculations, however, the rather poor agreement between the theoretical and experimental angular distributions for π^+ scattering results in substantially larger uncertainties in the extracted value of $\beta(\pi^+)$ than can be reflected in the quoted error. It is therefore premature to draw definite conclusions from the ARPIN analysis. Theoretical considerations also indicate only a slight preference for excitation of neutron particle-hole configurations, which would imply $\beta_3(\pi^-) \gtrsim \beta_3(\pi^+)$. The assumptions made are (1) the ^{208}Pb ground state is composed of fully-closed shells, (2) the 3^- state in ^{208}Pb can be described by the shell-model wave functions of True *et al.*,[38] and (3) the reaction amplitudes for each of the 24 neutron and 20 proton configurations in those wave functions are equal. Then, the further assumption of (3, 3) dominance results in a ratio $\beta_3(\pi^-)/\beta_3(\pi^+) = 1.02$ or 1.13, depending on the choice of phase between the pion-proton and pion-neutron terms. These simple estimates are consistent with the observation of similar values of $\beta_3(\pi^-)$ and $\beta_3(\pi^+)$ from the DWPI analyses, and the possible preference for neutron particle-hole configurations in the ARPIN analyses. Finally, from all of these considerations, it is clear that the large neutron excess in ^{208}Pb does not produce a strong enhancement for π^- scattering to the 3^- state.

V. SUMMARY

Elastic and inelastic scattering of both π^+ and π^- by Si, ^{58}Ni, and ^{208}Pb has been studied at $E_{lab} = 162$ MeV.[39] The angular distributions for elastic scattering are compared with first-order optical-model calculations and good agreement is obtained. Fits in configuration space using a Kisslinger form for the potential yield values of the parameters that do not seem to vary in a consistent manner for the different target nuclei. Calculations in momentum space show optimum agreement with the data if modifications to the parameters are included. These modifications affect the matter density radii (which may simulate the effect of neglected, higher-order terms, e.g., ρ^2 terms) and the local pion-nucleon energies (which may arise from the necessary but neglected Coulomb and binding energy corrections).

The use of a second-order optical potential which explicitly includes true absorption phenomena would be more appealing than the use of a first-order potential, as considered here. However, the relative success of the present calculations could indicate that the parametrizations of the radius and energy modifications may provide an important insight into future improvements of the pion-nucleus optical model.

The wave functions which were obtained for elastic scattering were employed in DWIA calculations of inelastic scattering using macroscopic form factors. The resulting angular distributions have both shapes and magnitudes consistent with the data. Differences between the configuration- and momentum-space methods of analysis are not completely understood and require further theoretical study.

ACKNOWLEDGMENTS

We acknowledge the cooperation and assistance of the staff of LAMPF and EPICS during the course of the experiment. We also wish to thank F. Karasek, D. Kurth, and B. Kazich for their help in this work. We are particularly grateful to Dr. F. Tabakin for useful discussions concerning the necessity of energy corrections in PIPIT and Dr. R. A. Eisenstein for providing a copy of the code DWPI. This work was performed under the auspices of the U. S. Department of Energy and was supported in part by the National Science Foundation.

[1] F. Binon, P. Duteil, J. P. Garron, J. Gorres, L. Hugon, J. P. Peigneux, C. Schmit, M. Spighel, and J. P. Stroot, Nucl. Phys. B17, 168 (1970).

[2] E. T. Boschitz in *Proceedings of the International Conference on High Energy Physics and Nuclear Structure, Zurich, 1977,* edited by M. P. Locher (Birkhauser, Basel, 1977), p. 133.

[3] J. Jansen, J. Zichy, J. P. Albanese, J. Arvieux, J. Bolger, E. Boschitz, C. H. Q. Ingram, and L. Pflug, Phys. Lett. 77B, 359 (1978).

[4] C. Lunke, R. Corfu, J.-P. Egger, P. Gretillat, J. Piffaretti, E. Schwarz, J. Jansen, C. Perrin, and B. M. Preedom, Phys. Lett. 78B, 201 (1978).

[5] S. Iverson, A. Obst, K. K. Seth, H. A. Thiessen, C. L. Morris, N. Tanaka, E. Smith, J. F. Amann, R. Boudrie, C. Burleson, M. Devereux, L. W. Swen-

son, P. Varghese, K. Boyer, W. J. Braithwaite, W. Cottingame, and C. Fred Moore, Phys. Rev. Lett. 40, 17 (1978).
[6]B. M. Preedom, R. Corfu, J. P. Egger, P. Gretillat, C. Lunke, J. Piffaretti, E. Schwarz, J. Jansen, and C. Perrin, Nucl. Phys. A236, 385 (1979).
[7]C. H. Q. Ingram, E. Boschitz, L. Pflug, J. Zichy, J. P. Albanese, and J. Arvieux, Phys. Lett. 76B, 173 (1978).
[8]C. A. Wiedner, J. A. Nolen, Jr., W. Saathoff, R. E. Tribble, J. Bolger, J. Zichy, K. Stricker, H. McManus, and J. A. Carr, Phys. Lett. 78B, 26 (1978).
[9]J. P. Egger, R. Corfu, P. Gretillat, C. Lunke, J. Piffaretti, E. Schwarz, C. Perrin, J. Jansen, and B.M. Preedom, Phys. Rev. Lett. 39, 1608 (1977).
[10]B. Zeidman, C. Olmer, D. F. Geesaman, R. L. Boudrie, R. H. Siemssen, J. F. Amann, C. L. Morris, H. A. Theissen, G. R. Burleson, M. J. Devereux, R. E. Segel, and L. W. Swenson, Phys. Rev. Lett. 40, 1539 (1978).
[11]H. A. Thiessen *et al.* (unpublished).
[12]E. Borie, Phys. Lett. 68B, 433 (1977).
[13]K. Boyer *et al.* (unpublished).
[14]P. J. Bussey, J. R. Carter, D. R. Dance, D. V. Bugg, A. A. Carter, and A. M. Smith, Nucl. Phys. B58, 363 (1973).
[15]J. Piffaretti, R. Corfu, J. P. Egger, P. Gretillat, C. Lunke, E. Schwarz, C. Perrin, and B. M. Preedom, Phys. Lett. 71B, 324 (1977).
[16]J. S. Blair, *Scattering of Strongly Absorbed Particles*, Boulder Lectures, Vol. 8C (University of Colorado Press, Boulder, 1966) p. 343.
[17]C. W. DeJager, H. DeVries, and C. DeVries, At. Data Nucl. Data Tables 14, 479 (1974).
[18]E. J. Moniz, Lectures from the Les Houches Summer School on Nuclear Physics with Heavy Ions and Mesons, July, 1977 (unpublished).
[19]M. D. Cooper and R. A. Eisenstein, LASL Report No. LA-6929 MS, 1975 (unpublished).
[20]L. S. Kisslinger, Phys. Rev. 98, 761 (1955).
[21]M. M. Sternheim and E. Auerbach, Phys. Rev. Lett. 25, 1500 (1970).
[22]D. J. Herndon, A. Barbaro-Galtieri, and A. H. Rosenfeld, Lawrence Radiation Laboratory Report No. UCRL-20030, 1970 (unpublished).
[23]M. M. Sternheim and K.-B. Yoo, Phys. Rev. Lett. 41, 1781 (1978).
[24]R. A. Eisenstein and F. Tabakin, Comput. Phys. Commun. 12, 237 (1976).
[25]R. Landau, S. Phatak, and F. Tabakin, Ann. Phys. (N.Y.) 78, 299 (1973).
[26]J. Londergan, K. McVoy, and E. Moniz, Ann. Phys. (N.Y.) 86, 147 (1974).
[27]L. C. Liu and C. M. Shakin, Phys. Rev. C 16, 1963 (1977).
[28]J. A. Nolen and J. P. Schiffer, Ann. Phys. Nucl. Sci. 19, 471 (1969); S. Shlomo and E. Friedman, Phys. Rev. Lett. 39, 1180 (1977); G. Dugan, S. Childress, L. M. Lederman, L. E. Price, and T. Sanford, Phys. Rev. C 8, 909 (1973).
[29]L. Ray, W. R. Coker, and G. W. Hoffmann, Phys. Rev. C 18, 2641 (1978).
[30]J. W. Negele and D. Vautherin, Phys. Rev. C 5, 1472 (1972).
[31]C. Olmer, B. Zeidman, D. F. Geesaman, T.-S. H. Lee, R. E. Segel, L. W. Swenson, R. L. Boudrie, H. A. Thiessen, and C. L. Morris, Phys. Rev. Lett. 43, 612 (1979).
[32]R. A. Eisenstein and G. A. Miller, Comput. Phys. Commun. 11, 95 (1976).
[33]D. S. Gale and J. S. Eck, Phys. Rev. C 7, 1950 (1973) and references therein; Y. Horikawa, Y. Torizuka, A. Nakada, S. Mitsunobu, Y. Kojima, and M. Kimura, Phys. Lett. 36B, 9 (1971).
[34]J. Kokame, K. Fukunaga, and H. Nakamura, Phys. Lett. 20, 672 (1966).
[35]D. A. Goldberg, S. M. Smith, H. G. Pugh, P. G. Roos, and N. S. Wall, Phys. Rev. C 7, 1938 (1973); G. Bruge, J. C. Faivre, H. Faraggi, and A. Bussiere, Nucl. Phys. A146, 597 (1970); M. B. Lewis, Nucl. Data Sheets B5, 243 (1971).
[36]H. Rebel, G. W. Schweimer, G. Schatz, J. Specht, R. Löhken, G. Hauser, D. Habs, and H. Klewe-Nebenius, Nucl. Phys. A182, 145 (1972); M. Inoue, *ibid.* A119, 449 (1968).
[37]T.-S. H. Lee and S. Chakravarti (unpublished).
[38]W. True, C. W. Ma, and W. T. Pinkston, Phys. Rev. C 3, 2421 (1971).
[39]See A. I. P. document no. PAPS PRVCA-21-xxx-24 for 24 pages of tabulations of the pion scattering cross sections reported here. Order by PAPS number and journal reference from: American Institute of Physics, Physics Auxiliary Publication Service, 335 E. 45th Street, New York, N. Y. 10017. The price is $1.50 for microfiche, or $5 for photocopies; airmail additional. Make checks payable to the American Institute of Physics. This material also appears in *Current Physics Microfilm*, the monthly microfilm edition of the complete set of journals published by A. I. P., on the frames immediately following this journal article.